Eur. Phys. J. A **2**, 311–322 (1998)

THE EUROPEAN PHYSICAL JOURNAL A

Phenomenological $\pi N \to \pi\pi N$ amplitude and the modelling of the Olsson–Turner and Chew–Low approaches

A.A. Bolokhov[1], S.G. Sherman[2]

[1] Sankt-Petersburg State University, Sankt-Petersburg, 198904, Russia (e-mail: bolokhov@niif.spb.su)
[2] St. Petersburg Institute for Nuclear Physics, Sankt-Petersburg, 188350, Russia (e-mail: sherman@hep486.pnpi.spb.ru)

Received: 10 December 1997
Communicated by V.V. Anisovich

Abstract. The phenomenological amplitude for the reaction $\pi N \to \pi\pi N$ fixed by fittings to the experimental data in the energy region $0.300 \leq P_{\rm Lab} \leq 500$ MeV/c is used for modelling the Chew–Low extrapolation and Olsson–Turner threshold approach. It is shown that the uncritical application of the former results in enermous theoretical errors, the extracted values being in fact random numbers. The results of the Olsson–Turner method are characterized by significant systematic errors coming from unknown details of the isobar physics.

PACS. 13.75.-n Hadron-induced low- and intermediate reactions and scattering (energy $\leq$10 GeV) – 13.75.Gw Pion-baryon interactions – 13.75.Lb Meson-meson interaction

1 Introduction

The reactions $\pi N \to \pi\pi N$ and $K \to \pi\pi e\nu$ are considered as the most important sources of the indirect information on the low energy characteristics of the $\pi\pi$ interaction predicted in the framework of the Chiral Perturbation Theory (ChPT) approach. The recent results [1] of so called Generalized ChPT approach [2] and the progress in the two–loop ChPT calculations [1, 3] are claiming for more precise experimental information on the $\pi\pi$ interaction at low energies.

The review of previously used methods of extracting the $\pi\pi$ characteristics from $\pi N \to \pi\pi N$ data and the details of their applications can be found in the paper [4] by Leksin. The methods suggested for application to the modern $\pi N \to \pi\pi N$ experiments are the following [5].

1. The Chew–Low extrapolation procedure by Goebel, Chew and Low [6] is an apparently model-independent approach. It can present a complete information on the $\pi\pi$ cross section, provided the OPE contribution dominates and the interval of the nucleon momentum transfer squared t_{NN}, which equals the squared mass of the virtual pion, allows a unique extrapolation. When comparing the phase space of momentum transfer $-20\mu^2 < t_{NN} < -0.2\mu^2$ at $P_{\rm Lab} = 500$ MeV/c with the distance of extrapolation $\approx \mu^2$, it becomes obvious that the $\pi N \to \pi\pi N$ kinematics itself does not prevent the use of the Chew–Low procedure at low energies, provided there are enough events. It is the presence of contributions like that of Δ and $N^{(*)}$ isobars which makes it difficult to perform a straightforward extrapolation at moderate energies due to the perturbation of the simple t_{NN}-dependence of the OPE graph. The absolute values of all other contributions are killed at the extrapolation point $t_{NN} = \mu^2$, but the result of extrapolation is known to be sensitive to the shape of the extrapolation curve [8, 4].

2. In view of importance of concurrent mechanisms at intermediate energies, the approach could be changed to determining the OPE parameters directly in the physical region of the reaction — this was implemented by the model of Oset and Vicente–Vacas [9]. It is clear that the neglect of a specific resonance contribution and/or the account of another one are capable to produce a lot of derivatives of the Oset–Vicente–Vacas model.

There is the energy region below $P_{\rm Lab} = 500$ MeV/c, where the variation of t_{NN} is sufficient to detect the OPE contribution, since the contributions of the concurrent processes, being non-negligent, are smooth enough. The relativistic model [10] takes these features into account and naturally completes the Oset–Vicente-Vacas approach in this specific energy domain.

3. The investigations by Olsson and Turner [11] are devoted to the threshold properties of $\pi N \to \pi\pi N$ reactions. Since the phase space of t_{NN} variable shrinks to the point $t^0_{NN} = -2.31\mu^2$, the application of the Chew–Low procedure is impossible. The idea is to take advantage of Chiral Dynamics at the $\pi N \to \pi\pi N$ threshold.

The important results of the approach are the formulae expressing the $\pi\pi$-scattering lengths in terms of the threshold characteristics of the pion-production reactions. These formulae gained a broad application, especially in the recent years, when new data on the $\pi N \to \pi\pi N$ reac-

tions in the close-to-threshold energy region became available [12, 13, 14, 15], [16], [17], [18].

The evidence of the importance of next-to-leading order terms of Chiral Lagrangian for the πN interaction and, in particular, for the $\pi N \to \pi\pi N$ amplitude [19], makes it necessary to modify the Olsson–Turner method. Recently the approach of heavy baryon approximation was used to derive corrections to the Olsson–Turner formulae and to make direct predictions of ChPT for the threshold $\pi N \to \pi\pi N$ amplitude itself [20].

The modern $\pi N \to \pi\pi N$ experiments planned to test the ChPT predictions are listed in [21]. Some of the experiments have been already finished: BNL and LAMPF results on total cross sections have been published [17], [18], 1D-distributions have appeared recently in WWW (home pages [22], [23]), higher distributions are in progress, the off-line treatment of experimental tapes of the TRIUMF experiment [24] will be completed soon. Therefore, it is time to discriminate between the above methods.

Recently the relativistic version of the Oset–Vicente-Vacas approach **2** was used for the analysis of the existing low-energy $\pi N \to \pi\pi N$ data. The basics of the model, the data base and major results of fittings are described in [25]. This paper uses the approach **2** since both the Chew–Low extrapolation and the Olsson–Turner threshold formulae cannot present any hint for cross-checking alternative methods. The phenomenological amplitude is fixed by fitting to the data on total cross sections and distributions in the energy region from the threshold up to $P_{\rm Lab} \leq 500$ MeV/c.

The main goal of the present work is to present grounds for comparison of the listed approaches **1**, **2**, **3**. Having determined the parameters of the phenomenological $\pi N \to \pi\pi N$ amplitude in the framework of the approach **2**, one can forget about parameter errors and use the theoretical amplitude as the original input to test the approaches **1** and **3**.

The paper is organized as follows. Necessary kinematical formulae are collected in Sect. 2. Section 3 deals with the model-independent properties of the $\pi N \to \pi\pi N$ amplitude at the threshold and describes the results of modelling the threshold data necessary for implementation of the Olsson–Turner approach. The results of the Chew–Low extrapolation applied to the simulated data are exposed and discussed in Sect. 4. The summary, concluding remarks and discussion of the further development are given in Conclusions.

2 General structure of $\pi N \to \pi\pi N$ Amplitude

This short section introduces the basic formulae of the paper [25].

We consider the reaction

$$\pi^a(k_1) + N_\alpha(p;\lambda_i) \to \pi^b(k_2) + \pi^c(k_3) + N_\beta(q;\lambda_f), \quad (1)$$

where $a,b,c = 1,2,3$ and $\alpha,\beta = 1,2$ are isotopic indices of pions and nucleons, respectively, and $\lambda_i(\lambda_f)$ are polarizations of initial (final) nucleons.

Separating the nucleon spinor wave functions from the reaction amplitude $M^{abc}_{\beta\alpha}(\lambda_f;\lambda_i)$

$$M^{abc}_{\beta\alpha}(\lambda_f;\lambda_i) = \bar u(q;\lambda_f)\hat M^{abc}_{\beta\alpha}(i\gamma_5)u(p;\lambda_i), \quad (2)$$

one can define the isoscalar amplitudes $\hat A, \hat B, \hat C, \hat D$ by

$$\hat M^{abc}_{\beta\alpha} = \hat A\tau^a_{\beta\alpha}\delta^{bc} + \hat B\tau^b_{\beta\alpha}\delta^{ac} + \hat C\tau^c_{\beta\alpha}\delta^{ab} + \hat D i\varepsilon^{abc}\delta_{\beta\alpha}, \quad (3)$$

τ^a, $a = 1,2,3$ being the nucleon-isospin generators.

Each isoscalar function A, B, C, D is decomposed into four independent spinor form factors in the following way:

$$\begin{aligned}\hat A &= S_A + \bar V_A\hat k + V_A\hat{\bar k} + i/2T_A[\hat k,\hat{\bar k}]\\ &\equiv \begin{pmatrix} S_A\\ \bar V_A\\ V_A\\ T_A\end{pmatrix}^T \cdot \begin{pmatrix} \hat 1\\ \hat k\\ \hat{\bar k}\\ i/2[\hat k,\hat{\bar k}]\end{pmatrix},\\ \hat B &= S_B + \bar V_B\hat k + \ldots,\\ &\ldots \quad .\end{aligned} \quad (4)$$

Here, k, $\bar k$ are the crossing-covariant combinations of pion momenta

$$k = -k_1 + \varepsilon k_2 + \bar\varepsilon k_3; \quad \bar k = -k_1 + \bar\varepsilon k_2 + \varepsilon k_3, \quad (5)$$

where $\varepsilon = \exp(2\pi i/3) = -1/2 + i\sqrt{3}/2$, $\bar\varepsilon = \varepsilon^* = -1/2 - i\sqrt{3}/2$. These combinations together with

$$Q = -k_1 + k_2 + k_3 = p - q, \quad P \equiv p + q \quad (6)$$

are used to define five independent scalar variables

$$\begin{aligned}&t_{NN} \equiv Q^2, \quad \theta \equiv Q\cdot k = \theta_R + i\theta_I, \quad \bar\theta \equiv Q\cdot\bar k = \theta_R - i\theta_I,\\ &\nu \equiv P\cdot k = \nu_R + i\nu_I, \quad \bar\nu \equiv P\cdot\bar k = \nu_R - i\nu_I,\end{aligned} \quad (7)$$

determining the point in the phase space of the considered reaction.

The four-pion vertex $V_{4\pi}$ of the OPE graph is characterized by the Mandelstam variables. To avoid the off-shell ambiguity we use only the two-pion invariant mass

$$s_{\pi\pi} \equiv (k_2 + k_3)^2 \quad (8)$$

in the discussion below.

The matrix element $\|M\|^2$ entering the unpolarized cross section is the quadratic form of the vector of spinor structures $(S_X, \bar V_X, V_X, T_X)$:

$$\begin{aligned}\|M_X\|^2 &\equiv 1/2\sum_{\lambda_f,\lambda_i}\left[\bar u(q;\lambda_f)\hat M_X(i\gamma_t)u(p;\lambda_i)\right]\\ &\quad\times\left[\bar u(q;\lambda_f)\hat M_X(i\gamma_5)u(p;\lambda_i)\right]^*\\ &= \begin{pmatrix} S_X\\ \bar V_X\\ V_X\\ T_X\end{pmatrix}^\dagger G \begin{pmatrix} S_X\\ \bar V_X\\ V_X\\ T_X\end{pmatrix},\\ &\quad (X = \{\pi^-\pi^+n\},\{\pi^-\pi^0p\},\{\pi^0\pi^0n\},\\ &\quad \{\pi^+\pi^+n\},\{\pi^+\pi^0p\}),\end{aligned} \quad (9)$$

$$G \equiv \frac{1}{2} Sp \left[(\hat{q}+m) \left\{ \begin{array}{c} \hat{1} \\ \hat{k} \\ \hat{\tilde{k}} \\ \frac{i}{2}[\hat{k},\hat{\tilde{k}}] \end{array} \right\} (\hat{p}-m)\gamma_0 \left\{ \begin{array}{c} \hat{1} \\ \hat{k} \\ \hat{\tilde{k}} \\ \frac{i}{2}[\hat{k},\hat{\tilde{k}}] \end{array} \right\}^{\dagger} \gamma_0 \right]. \tag{10}$$

The hermitian matrix G is given in the paper [10] for the simplified case of equal pion masses.

To plot the data and theoretical results we define the "quasi-amplitude" $\langle M \rangle_{(\alpha)}$, which is the square root of the cross section $\sigma_{(\alpha)}(\|M\|^2)$ divided by the phase space $\sigma^{psv}_{(\alpha)} \equiv \sigma_{(\alpha)}(1)$:

$$\langle M \rangle_{(\alpha)} \equiv \sqrt{\frac{\sigma_{(\alpha)}(\|M\|^2)}{\sigma_{(\alpha)}(1)}}. \tag{11}$$

Here, the phase space $\sigma(1)$ is the theoretical cross section calculated with the unit matrix element.

3 Olsson–Turner approach

The idea of the Olsson–Turner approach was to relate the threshold values of the $\pi N \to \pi\pi N$ amplitude with the $\pi\pi$-scattering lengths. We advise reader to look for details into the original papers [11]. Here, we only remind that there are two principal steps in the discussed approach **1)** determination of the threshold limits of amplitudes for independent isospin channels; **2)** calculation of the $\pi\pi$-scattering lengths with the account of other contributions, like isobar exchanges, to the above threshold limits. These steps are vital for the success of the approach, and our conclusions are based upon the analysis of these steps.

3.1 Threshold amplitudes

To discuss the first step one needs to derive the model-independent properties of the reaction amplitude at the very threshold and to judge upon the quality of experimental information.

There are considerable simplifications in the representation of the $\pi N \to \pi\pi N$ amplitude (4) at the threshold of the reaction. The simplifications arise from a) the coincidence of momenta of the outgoing pions ($\hat{k}_2 = \hat{k}_3$), b) the vanishing contribution of the isospin-antisymmetric amplitudes $\hat{D}$ and $\hat{B} - \hat{C}$ (see (3)).

Another simplification appears after summing over final polarizations and averaging over initial ones of the amplitude (2) squared modulus. It degenerates at the threshold to

$$\|M_X\|^2 = (-t^0_{NN})|S^0_X - (2m+3\mu)(\bar{V}^0_X + V^0_X)|^2, \tag{12}$$
$$(X = \{\pi^-\pi^+n\}, \{\pi^-\pi^0p\}, \{\pi^0\pi^0n\}, \{\pi^+\pi^+n\}, \{\pi^+\pi^0p\}),$$

where $t^0_{NN} = -3\mu^2 m/(m+2\mu)$ is the threshold value of the variable t_{NN}. This represents the grounds to introduce the *threshold amplitudes*.

The isotopic threshold amplitudes are

$$\begin{aligned} A^0 &= \sqrt{-t^0_{NN}}\,[S^0_A - (2m+3\mu)(\bar{V}^0_A + V^0_A)], \\ B^0 &= \sqrt{-t^0_{NN}}\,[S^0_B - (2m+3\mu)(\bar{V}^0_B + V^0_B)], \\ C^0 &= \sqrt{-t^0_{NN}}\,[S^0_C - (2m+3\mu)(\bar{V}^0_C + V^0_C)], \end{aligned} \tag{13}$$

where all form factors are to be calculated at the threshold values of kinematical variables; this provides

$$B^0 = C^0. \tag{14}$$

To link the isotopic threshold amplitudes (13) with the experimental information let us construct the quantities M^0

$$\begin{aligned} &M^0_{\{-+n\}} = (A^0 + B^0)\sqrt{2}/2,\ M^0_{\{-0p\}} = B^0/2. \\ &M^0_{\{00n\}} = A^0/2,\ M^0_{\{++n\}} = B^0,\ M^0_{\{+0p\}} = B^0/2, \end{aligned} \tag{15}$$

which include both the isotopic and the statistical factors (hereafter, we use meson charges in notations for the reaction channels).

Then the absolute values of the threshold amplitudes M^0_X can be expressed in terms of threshold limits of the experimental quasi-amplitudes $\langle M_X \rangle$ defined by eq. (11):

$$\begin{aligned} &|M^0_X| = \langle M_X \rangle_{|s \to s_0}, \\ &(X = \{-+n\}, \{-0p\}, \{00n\}, \{++n\}, \{+0p\}). \end{aligned} \tag{16}$$

The threshold amplitudes (15) are not dimensionless; their numerical values will be given in $(\mathrm{GeV})^{-1}$.

The threshold limits (15), determined by two isotopic threshold amplitudes A^0 and B^0 only, must satisfy three relations. The first two are straightforward:

$$|M^0_{\{++n\}}| = 2|M^0_{\{-0p\}}| = 2|M^0_{\{+0p\}}|. \tag{17}$$

It follows from the definition (15) that

$$M^0_{\{++n\}} = \sqrt{2}\, M^0_{\{-+n\}} - 2M^0_{\{00n\}}. \tag{18}$$

This implies that the relation between positive quantities (16) can be either

$$|M^0_{\{++n\}}| = \sqrt{2}|M_{\{-+n\}}| - 2|M^0_{\{00n\}}| \tag{19}$$

or

$$|M^0_{\{++n\}}| = \sqrt{2}|M^0_{\{-+n\}}| + 2|M^0_{\{00n\}}| \tag{20}$$

or

$$|M^0_{\{++n\}}| = -\sqrt{2}|M^0_{\{-+n\}}| + 2|M^0_{\{00n\}}|, \tag{21}$$

depending on relative sign of A^0 and B^0.

Now it is necessary to recall the known properties of $\pi N \to \pi\pi N$ cross sections. Since in the vicinity of the threshold the known cross sections $\sigma_{\{00n\}}$ of the $\{00n\}$ channel are approximately equal to the cross sections

$\sigma_{\{-+n\}}$, this excludes the possibility given by (19), because it results in the negative right-hand side. The cross sections $\sigma_{\{++n\}}$ are considerably smaller than $\sigma_{\{-+n\}}$ and $\sigma_{\{00n\}}$ at $P_{\rm Lab} \leq 0.5\,{\rm GeV/c}$; so the variant (20) is also impossible. Thus, we can state, combining with the previous two relations, that

$$2|M^0_{\{-0p\}}| = 2|M^0_{\{+0p\}}| = |M^0_{\{++n\}}| = 2|M^0_{\{00n\}}| - \sqrt{2}|M^0_{\{-+n\}}|. \qquad (22)$$

Apart from the neglect of imaginary parts, the obtained relations (22) are model-independent, since only the symmetry arguments and few properties of experimental cross sections were used. There is a strong motivation to consider the parameters A^0 and B^0 as real ones. Indeed, the value of the imaginary part collects contributions which are due to the following:

a. Three-particle intermediate states. This includes contributions of quasi-two-particle states, when the third particle is present as a spectator, namely, N for the $\pi\pi$ state and π for the πN state; the former configuration is characterized by the large imaginary part of isospin-zero $\pi\pi$ amplitude. The three-particle phase space makes this contribution vanish at the threshold. It was verified with the use of $(1/m)$ expansion in the paper [20] that $\pi\pi$ loops did not contribute to the threshold $\pi N \to \pi\pi N$ amplitude.

b. Two-particle intermediate states. Only the πN system is allowed at the considered energies. The angular momentum conservation forces these particles to be in the P wave when the final particles are in the S wave at threshold, according to quantum mechanics; otherwise, the P-parity properties of the πN system mismatch those of the $\pi\pi N$ final state. The known phases of the P_{31} ($\approx -4^\circ$) and P_{11} ($\approx 2^\circ$) waves of the πN-elastic amplitudes approve the neglect of the imaginary part of the $\pi N \to \pi\pi N$ amplitude at the threshold.

c. Single-particle intermediate states. The only possible one at the threshold of the $\pi N \to \pi\pi N$ reaction is the Δ isobar. It appears in the P wave of initial particles, and its decay into the threshold configuration of the final $\pi\pi N$ state has negligible width [26].

The estimate of the imaginary part of the $\pi N \to \pi\pi N$ amplitude by the dispersion analysis of the paper [27] allows us to consider the amplitude to be approximately real up to the energies $P_{\rm Lab} = 0.50$ GeV/c. Thus, there should be no expectations for finding a physically meaningful imaginary part or, a nontrivial relative phase of A^0 and B^0, at the $\pi N \to \pi\pi N$ threshold. Hence, the threshold identity (21) must be practically exact. The identities (17) are the exact consequences of the isotopic invariance irrespective of the value of the imaginary part.

The original formulae [11] by Olsson and Turner express five threshold amplitudes in terms of two $\pi\pi$-scattering lengths $a_0^{I=0}$ and $a_0^{I=2}$ in the form

$$M^0_X = c^0_X a_0^{I=0} + c^2_X a_0^{I=2} + \tilde{c}_X, \qquad (23)$$
$$(X = \{-+n\}, \{-0p\}, \{00n\}, \{++n\}, \{+0p\}).$$

The numerical values of coefficients c^0_X, c^2_X, $\tilde{c}_X$ given by Olsson and Turner satisfy the conditions (22) exactly.

To resume, one can state that the threshold limits of quasi-amplitudes of five channels contain independent information on two isotopic threshold amplitudes only. The relations (22) are powerful consistency constraints on the experimental input of the Olsson–Turner approach.

The examination of relations (15), (16) shows that, apart from the overall sign ambiguity of isotopic threshold amplitudes A^0, B^0, their relative sign can also become indefinite, depending on the accuracy of experimental information. In what follows we call the solution *physical* (*unphysical*), when A^0 and B^0 are of different (equal) signs. In terms of the $\pi\pi$-scattering lengths, the two opposite signs correspond to the different (equal) signs of $a_0^{I=0}$ and $a_0^{I=2}$.

3.2 Test of consistency of the threshold data

The advantage of the Olsson–Turner approach is the simplicity of experimental information the approach relies upon. One needs to know only the threshold limits of quasi-amplitudes (11). The latter are extrapolated from data on total cross sections which are the most reliable statistically.

The results of global analyses have been already reported starting from the publication [28] (see also [29]). The most important conclusion of the work [28] is that the data from the region $P_{\rm Lab} \leq 400$ MeV/c admit amplitudes which are linear in energy of the center-of-mass system. Here, the data with $P_{\rm Lab} \leq 500$ MeV/c will be exposed to linear fittings. Moreover, any preliminary selection will be excluded. Indeed, it is the unmotivated preference of one set of data to another that is the reason for contradictory results.

The entire data base described in Sect. 3 of the paper [25] contains, along with the old data, the relatively new results. It should be noted, that before the OMICRON measurements [13, 14, 15] only the data of the $\{-+n\}$ channel allowed one to obtain the definite results from the linear fit; the above mentioned OMICRON data provided the possibility to carry out linear fittings for the $\{-0p\}$ and $\{++n\}$ channels as well. The authors of the paper [28] took advantage of the precise data [17] on $\sigma_{\{00n\}}$ very close to threshold and provided the simultaneous linear fit of all channels.

Recent experimental information given in [18] for the first time makes it possible to determine the threshold limit of the cross section for the channel $\{+0p\}$ and to test the prediction (22) for the relation

$$M^0_{\{+0p\}} = M^0_{\{-0p\}}. \qquad (24)$$

In fact, the approximate equality of cross sections of these two channels is displayed along all energy interval considered.

We pay special attention to the $\{++n\}$ channel. There are two sets of the near-threshold data for the channel $\{++n\}$, namely, [14] and [16], which are in certain disagreement. They lead to different threshold limits $|M^0_{\{++n\}}|$.

Table 1. Threshold values provided by data fittings in the variants: ALL — all data; TRI — without [14]; OMI — without [16]; X — without [14, 16]; IND — independent fits of channels. Bold-face numbers correspond to physical solutions of real fits with seven free parameters, slanted ones relate to unphysical solutions. The roman-font numbers stand for fits with complex amplitudes. The numbers in brackets in the columns of the $\{-+n\}$ and $\{00n\}$ channels display the imaginary part of the resulting amplitude, provided B^0 is real. The last two rows represent predictions of eqs. (21) and (17) based on the data of individual fits for channels $\{-+n\}$, $\{00n\}$ and $\{-0p\}$

Fit	$\{-+n\}$ $\lvert A^0+B^0\rvert/\sqrt{2}$	$\{00n\}$ $\lvert A^0\rvert/2$	$\{-0p\}$ $\lvert B^0\rvert/2$	$\{+0p\}$ $\lvert B^0\rvert/2$	$\{++n\}$ $\lvert B^0\rvert$	$\chi^2_{\rm DF}$
ALL	**398 ± 18**	**413 ± 12**	**132 ± 6**	**132 ± 6**	**264 ± 11**	**0.99**
	524 ± 24	*252 ± 12*	*118 ± 5*	*118 ± 5*	*236 ± 11*	*1.56*
	401 ± 150	409 ± 101	132 ± 6	132 ± 6	264 ± 11	1.00
	(74 ± 123)	(52 ± 87)				
TRI	**404 ± 18**	**406 ± 12**	**121 ± 6**	**121 ± 6**	**241 ± 11**	**0.78**
	518 ± 24	*260 ± 12*	*106 ± 6*	*106 ± 6*	*212 ± 11*	*1.33*
	406 ± 26	406 ± 18	119 ± 6	119 ± 6	238 ± 12	0.77
	(10^{-4})	(10^{-4})				
OMI	**372 ± 23**	**447 ± 13**	**184 ± 10**	**184 ± 10**	**368 ± 20**	**0.83**
	533 ± 32	*241 ± 13*	*136 ± 10*	*136 ± 10*	*272 ± 20*	*1.60*
	401 ± 60	410 ± 54	197 ± 11	197 ± 11	395 ± 22	0.80
	(181 ± 23)	(128 ± 16)				
X	**387 ± 26**	**427 ± 14**	**154 ± 12**	**154 ± 12**	**307 ± 24**	**0.76**
	506 ± 36	*275 ± 14*	*83 ± 12*	*83 ± 12*	*166 ± 24*	*1.36*
	402 ± 98	410 ± 76	164 ± 14	164 ± 14	329 ± 29	0.76
	(154 ± 40)	(109 ± 28)				
IND	**401 ± 19**	**409 ± 18**	**155 ± 25**	**97 ± 51**	**263 ± 11**	ALL
					237 ± 12	TRI
					429 ± 26	OMI
					358 ± 37	X
Eq.(21)	–	–	**125 ± 22**	**125 ± 22**	**250 ± 44**	
Eq.(17)	–	–	–	**155 ± 25**	**310 ± 50**	

Four basic variants of fitting ALL, OMI, TRI and X were used for determination of the threshold amplitudes. These notations stand for the corresponding data selection and are described in the caption of Table 1. The auxiliary fits of the variant IND help to understand the trend dictated by data of individual channel in the simultaneous fit.

There were two types of fits in all four basic variants. First, the independent threshold values A^0 and B^0 are treated as being real. We use seven parameters for simultaneous linear fittings of five channels: two independent parameters for threshold values, A^0 and B^0, and five independent slopes in the invariant kinetic energy

$$T_{\rm K} = \sqrt{s} - T_0. \tag{25}$$

In calculations, the latter quantity was taken to be $T_{\rm K} = \sqrt{(p+k_1)^2} - (m_f + \mu_2 + \mu_3)$, since isospin splitting in the particle masses cannot be processed as a correction because of the nonanalytic mass-dependence of the near-threshold phase space — the demonstration can be found in [30].

Second, we add one parameter to describe the relative phase of the complex quantities A^0 and B^0.

The experimental data described in the paper [25] and the results of the main solution for the variant ALL are shown in Fig. 1, where the values of quasi-amplitudes $\langle M_X \rangle$ are plotted versus the invariant kinetic energy $T_{\rm K}$. The threshold amplitudes $|M_X^0|$ are collected in Table 1.

Every time there appeared another solution of the fit, the slanted numbers being used for resulting values in Table 1. It originates from the sign ambiguity discussed in Subsect. 3.1. These auxiliary solutions choose the relation (20) to be true one, and it was called *unphysical*, since it provides equal signs for isospin-zero and isospin-two $\pi\pi$-scattering lengths.

Let us compare the results of the linear fit discussed here with the results of the global analysis of the paper [25]. It is sufficient to compare Fig. 2 of [25] with Fig. 1 of this paper.

One can conclude that the threshold limits provided by the linear fit are good for all channels but the $\{-+n\}$ one. Because of the perceptible curvature revealed by solutions for the latter channel, the linear fit generally underestimates the value in question.

Table 1 does not allow one to choose a preferable solution using the χ^2 criterion. All solutions are practically on equal footing. Even the unphysical ones cannot be formally rejected.

The relatively low χ^2 values for the unphysical solution are first of all due to rather large overall uncertainties of experimental data. More discouraging reason is the

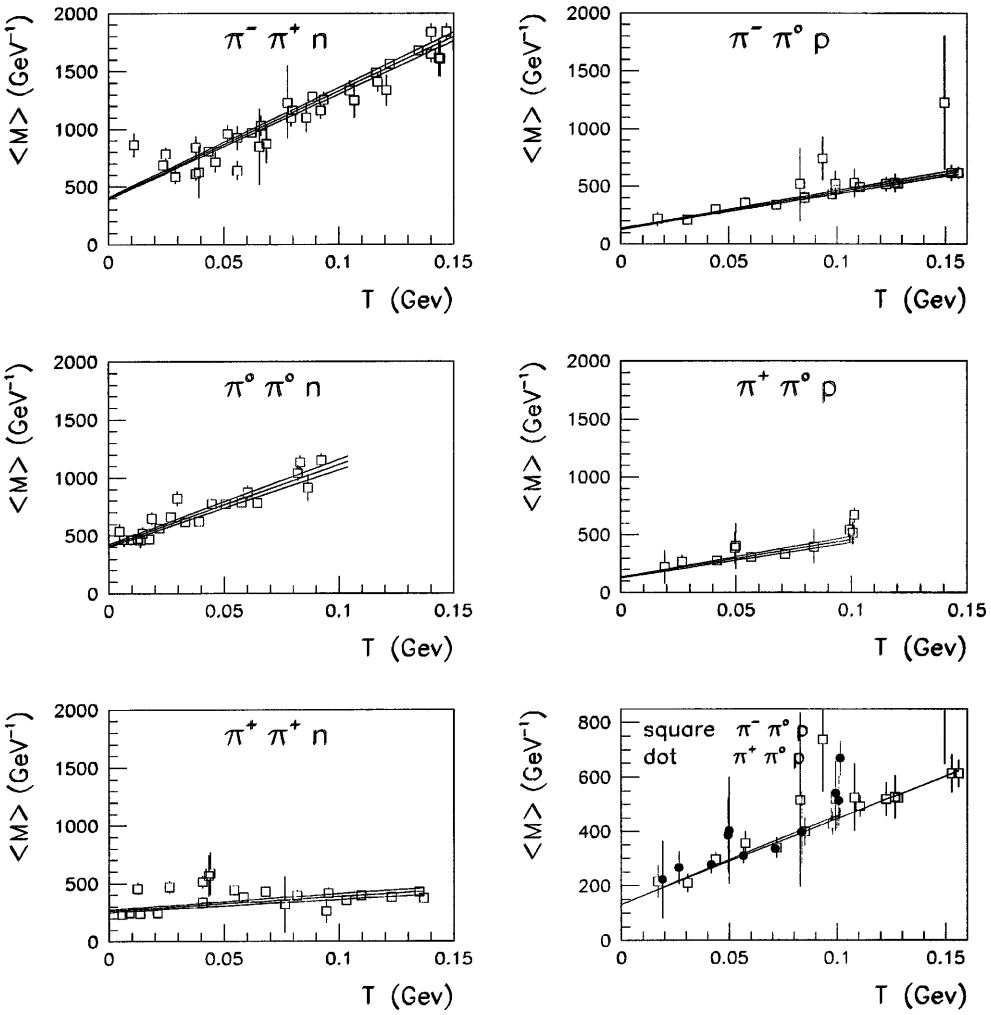

Fig. 1. Linear fit of total cross sections for all five channels with 7 free parameters

existence of subsets of data, supporting the discussed solution almost in every channel — compare IND results and the slanted numbers in Table 1. Only the data for the $\{00n\}$ channel reject this solution as a whole. Examination of the definitions (15) displays that, with the value B^0 no less than $200\,\mathrm{GeV}^{-1}$ fixed by the data for $\{-0p\}$ and $\{++n\}$ channels, the threshold limits for $\{-+n\}$ and $\{00n\}$ channels cannot be in balance, provided A^0 and B^0 amplitudes are of equal signs. Although the closest to threshold points of the OMICRON experiment [14] agree well with the large value of $|M^0_{\{-+n\}}|$, the data for the $\{00n\}$ channel [17] are incompatible with so small prediction given by the unphysical solution (see Table 1).

In all variants the presence of the imaginary part improves the fit. In the variants ALL and TRI the imaginary part Im A^0 remains compatible with zero: 104 ± 174 — ALL and $10^{-3} \pm 10^2$ — TRI (the amplitude B^0 is real). In the rest variants the imaginary part is found to be unreasonably large: 255 ± 32 — OMI, 218 ± 57 — X. Nevertheless, it cannot help to get rid of the contradiction between the data of the $\{-0p\}$ and $\{++n\}$ channels, especially in the OMI variant of the individual fit.

The examination of the threshold identities (17), (21) clearly displays the contradiction between the OMICRON data for $\{-0p\}$ and $\{++n\}$ channels themselves. Therefore, it was an inconsistent input of the OMICRON analysis [13]–[15] that produced controversial values of the $\pi\pi$-scattering lengths. The analysis given in Table 1 leads to the main conclusions that the threshold amplitudes given by the TRI and ALL variants are the most consistent from the point of view of the threshold identities and stability against the addition of the complex phase and definitely better χ^2 for physical solutions.

3.3 Account of nonOPE contributions

The threshold amplitudes discussed above are the corner stone for the Olsson–Turner approach. The general form of relations between the $\pi\pi$-scattering lengths with the threshold amplitudes is reproduced by (23). The quantities $\tilde{c}_X$ in these relations are corrections originating from the higher-order terms in the four-pion vertex of the OPE graph and from contributions of all other mechanisms (we call these latter *nonOPE*).

The calculation of coefficients c^0_X, c^2_X, $\tilde{c}_X$ was initially performed in the papers [11] in the approximation which is now identified with the leading order of ChPT.

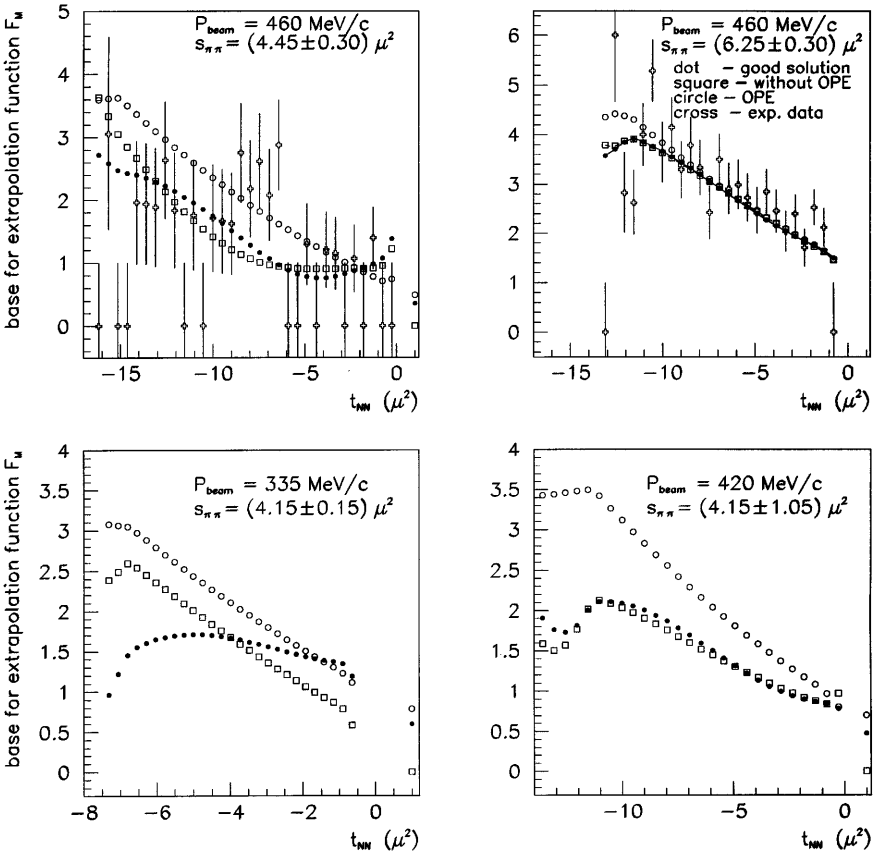

Fig. 2. Simulations of extrapolation data (F_M): *dot* — the amplitude of the best physical solution; *square* — the amplitude without the OPE contribution; *circle* — the pure OPE amplitude; *cross* — the available experimental data of the paper [38] by Blokhintseva

The improved formulae take into account the next-to-leading order terms of the Chiral πN lagrangian [31, 20]. The papers [32, 33, 34] deal with various schemes of accounting for the above terms in the framework of ChPT and/or Heavy Baryon ChPT and give the predictions for the nonrelativistic quanties D_1 and D_2, which coincide, up to a factor, with the threshold amplitudes A^0 and B^0:

$$\left\{ \begin{array}{c} D_1 \\ D_2 \end{array} \right\} = -\frac{\sqrt{\frac{2m}{m+E_0}}}{4m\sqrt{-t^0_{NN}}} \left\{ \begin{array}{c} B^0 \\ A^0 \end{array} \right\}. \qquad (26)$$

The difference in the predicted values, which are quoted in Table 2, makes it important to test the approximation schemes of the discussed papers and the hypotheses about the significance of various contributions. The results of analysis given in the paper [25] are suitable for this purpose, since the phenomenological amplitude determined by fittings in consistent with the treated data.

Table 2 contains the list of nonzero contributions to the threshold quantities D_1 and D_2 found in the solution with $\chi^2_{\rm DF} = 1.16$. The labels A_i are used for contributions of background parameters; g_i for OPE parameters; N_i for parameters of $\pi\pi NN$ interaction; Δ_i for parameters of $\pi N\Delta$, $\pi\pi N\Delta$ vertices; R_i for parameters of $\pi NN^{(*)}$, $\pi N^{(*)}\Delta$, $\pi\pi NN^{(*)}$ interactions and r_i for parameters of $\pi\rho NN$ vertex. We also quote the predictions of papers [32, 33, 34] and the results of the linear fit for the ALL and TRI data selections from Table 1 for comparison. The underestimate of D_2 by linear fits ALL and TRI is due to the above-mentioned perceptible deviation of the solution for $\{-+n\}$ channel from the linear pattern.

It should be noted that there is no absolute value of separate contributions because of the field redefinition freedom. However, the mass-on-shell parameters g_0, g_1, g_2 and g_3 of the four-pion vertex are stable, and the $\pi\pi$-scattering lengths are well defined in our approach though the "off-shell" contributions of the parameters g_0, g_1, g_2 and g_3 in Table 2 are model-dependent. Hence, the most general inferences which can be derived from this Table are the following:

1. The resulting quantities D_1 and D_2 are rather small differences of large contributions of various mechanisms.

2. The OPE mechanism meets the strong competition with all the rest ones in the threshold amplitudes, Δ being of importance for D_1, while $N^{(*)}$ is important for D_2.

3. The influence of the D-wave parameters g_2, g_3 is not negligible; their contribution reaches 30% of the total OPE contribution to both quantities D_1 and D_2.

3.4 Conclusion

As was seen in the previous subsection, to overcome the ambiguity in two threshold amplitudes A^0 and B^0, which the Olsson–Turner approach is relying upon, one should improve the accuracy of the experimental data on $\pi N \to \pi\pi N$ total cross sections. We noticed the evidence of the inapplicability of the linear fit for the $\{-+n\}$ channel (see Subsect. 3.2.) — this enlarges the systematic er-

Table 2. Contributions to the values D_1 and D_2 (in GeV^{-3})

	D_1			D_2		
A_1	310.80	±	35.44	310.80	±	35.44
A_2	194.66	±	6.66	194.66	±	6.66
A_3	531.15	±	13.61	−1062.31	±	27.23
A_4	597.88	±	21.26	1195.77	±	42.52
A_6	−35.15	±	95.36	−35.15	±	95.36
A_{12}	−69.56	±	8.05	−69.56	±	8.05
A_{13}	−312.40	±	7.48	624.80	±	14.96
A_{15}	−159.25	±	4.08	318.50	±	8.17
A_{16}	−186.93	±	16.28	−186.93	±	16.28
A_{17}	−170.52	±	21.80	341.04	±	43.60
g_1	102.14	±	251.12	102.14	±	251.12
g_2	488.02	±	31.38	−976.04	±	62.76
g_3	−101.07	±	33.53	−101.07	±	33.53
g_4	−161.90	±	32.09	323.80	±	64.19
r_2	300.89	±	7.75	−601.78	±	15.50
Δ_1	−46.75	±	15.48	93.50	±	30.96
Δ_2	−238.69	±	51.93	42.32	±	55.87
Δ_3	93.27	±	23.77	−186.54	±	47.53
Δ_4	−14.91	±	66.48	−115.75	±	133.00
Δ_5	5.88	±	11.12	−19.53	±	33.28
R_1	52.87	±	108.57	−1079.45	±	192.22
R_3	65.55	±	26.58	−131.09	±	53.15
R_5	0.46	±	12.95	−90.90	±	19.91
R_6	2.41	±	211.45	28.60	±	505.56
R_7	−7.91	±	4.73	−40.14	±	48.72
N_2	128.70	±	32.77	2.81	±	22.75
N_3	152.34	±	45.49	−304.69	±	90.97
N_5	−12.29	±	22.62	15.16	±	21.78
Sum	313.92	±	101.37	−1407.03	±	229.23
[32]	339.69	±	28.63	−1186.96	±	123.64
[33]	344.89	±	31.24	−1179.15	±	136.66
[34]	334.48	±	13.01	−1231.21	±	7.81
ALL	327.78	±	14.90	−1025.54	±	29.80
TRI	300.46	±	14.90	−1008.16	±	29.80

rors of A^0 and B^0 values. Here, one can see that there are unknown systematic errors in the theoretical field as well. A large amount of information on the isobar physics in necessary to fill this gap. Therefore, the approach is losing the advantage of simplicity that made it so attractive. Moreover, in view of importance of the D-wave parameters, the approach cannot be considered as an independent source of information on the $\pi\pi$ interaction, since it represents only two distinct quantities for the determination of four parameters.

4 Chew–Low extrapolation

The existence of the pole in the OPE contribution at $t_{NN} = \mu^2$ is the keystone for the Chew–Low approach. When plotting the experimental t_{NN} distributions in terms of cross-sections multiplied by $(t_{NN} - \mu^2)^2$, one can eliminate all contributions but the OPE one by extrapolation to the pole. The extrapolation result coincides, up to a factor, with the $\pi\pi$ cross section. However, there are several routines for the extrapolation to the point $t_{NN} = \mu^2$ — relevant discussion on the applications of the approach can be found in the review paper [4] (see also [35] for the phenomenological introduction); the tests of some variants performed long time ago were reported in the paper [36]. Only the linear extrapolation was found capable to provide definite results. This common feature of all applications of the Chew–Low procedure originates from the poor accuracy of data. The amplitudes obtained in our fittings present the possibility to test the approach by modelling the experimental data and to arrive to conclusions which are independent of the finite precision of the input.

4.1 Extrapolation function

From the very beginning it has become evident that the extrapolation function constructed in terms of the total cross section could represent a base neither for the linear nor for quadratic extrapolation, with the only exception for $\pi N \to \pi\pi N$ amplitude built of a constant OPE term plus a constant in the same spinor structure S. Therefore, we consider the extrapolation function $F_M(t_{NN})$, defined by the quasi-amplitude $\sqrt{d\sigma(\|M\|^2)/d\sigma(1)}$:

$$[F_M(t_{NN})]^2 \equiv \frac{(t_{NN}-\mu^2)^2}{(-t_{NN})(2g_{\pi NN})^2} \times \frac{d\sigma(\|M\|^2)}{d\sigma(1)}. \quad (27)$$

The principal feature of this extrapolation function is related to the assumption that the cross section vanishes at $t_{NN} = 0$ (see the discussion in Sect. 4.3.).

According to the general idea of the Chew-Low extrapolation that only the OPE term of the $\pi N \to \pi\pi N$ amplitude contributes to $F_M(\mu^2)$, it is convenient to define the auxiliary function

$$[F_{\mathrm{OPE}}(t_{NN}]^2 \equiv \frac{(t_{NN}-\mu^2)^2}{(-t_{NN})(2g_{\pi NN})^2} \times \frac{d\sigma(\|M_{\mathrm{OPE}}\|^2)}{d\sigma(1)} = \frac{\int\limits_{\Omega\,(t_{NN})} \int d\theta_I d\nu_I |V_{4\pi}|^2}{\int\limits_{\Omega\,(t_{NN})} \int d\theta_I d\nu_I}. \quad (28)$$

The quantities appearing in (27), (28) depend on the center-of-mass energy squared s and the two-pion invariant mass $s_{\pi\pi}$, which are fixed in the extrapolation; the amplitude M_{OPE} is obtained from M by eliminating all the contributions but the OPE one.

Analytical calculation of $F_M(t_{NN})$ is possible for the simplest amplitudes only. Therefore, we calculate numerically the function $F_M(t_{NN})$ obtained in various solutions for our phenomenological amplitude. However, because of the collapse of the integration domain $\Omega(t_{NN})$ outside the phase space of the $\pi N \to \pi\pi N$ reaction, the numerical calculation of the function $F_M(t_{NN})$ at $t_{NN} = \mu^2$ also becomes impossible. The Monte-Carlo utilities of high energy physics cannot generate events for the numerical integration outside the phase space.

The integration in the right-hand side of (28) results in the rational function of t_{NN} and $s_{\pi\pi}$. Neglecting the imaginary part of the OPE amplitude, one can treat this function as the quadratic form of the OPE parameters g_0, g_1, g_2, g_3 defined in the paper [10]:

$$[F_{\rm OPE}]^2 = \begin{pmatrix} g_0 \\ g_1 \\ g_2 \\ g_3 \end{pmatrix}^T (\hat{\Phi}) \begin{pmatrix} g_0 \\ g_1 \\ g_2 \\ g_3 \end{pmatrix}, \qquad (29)$$

where the symmetric matrix $\hat{\Phi}$ is explicitly given by

$$\begin{aligned}
&\Phi_{00} = 2,\ \Phi_{01} = \theta_R,\ \Phi_{02} = 2(9\theta_R^2 + A_1)/9,\\
&\Phi_{03} = (9\theta_R^2 - A_1)/9,\\
&\Phi_{11} = (3\theta_R^2 + A_1)/6,\ \Phi_{12} = (9\theta_R^2 + A_1)\theta_R/9,\\
&\Phi_{13} = (9\theta_R^2 - 7A_1)\theta_R/18,\\
&\Phi_{22} = 2(45\theta_R^4 + 10\theta_R^2 A_1 + A_1^2)/45,\\
&\Phi_{23} = (45\theta_R^4 - A_1^2)/45,\\
&\Phi_{33} = (45\theta_R^4 + 50\theta_R^2 A_1 + A_1^2)/90,\\
&A_1 = \frac{s_{\pi\pi} - 4\mu^2}{s_{\pi\pi}}[(\theta_R - t_{NN})^2 - 9 s_{\pi\pi}\tau/4],\\
&\theta_R = (t_{NN} + 3\mu^2 - 3s_{\pi\pi})/4. \qquad (30)
\end{aligned}$$

The discussed function (28) is well defined outside the reaction phase space, and it gives the value in question $F_{\rm OPE}(\mu^2) = F_M(\mu^2)$ at $t_{NN} = \mu^2$.

The calculations were performed with the function $\tilde{F}_{\rm OPE}(t_{NN})$ defined as follows:

$$[\tilde{F}_{\rm OPE}(t_{NN})]^2 \equiv \frac{\int\limits_{s_{\pi\pi}-\Delta s_{\pi\pi}}^{s_{\pi\pi}+\Delta s_{\pi\pi}} ds_{\pi\pi} \sqrt{\frac{s_{\pi\pi}-4\mu^2}{s_{\pi\pi}}} [F_{\rm OPE}(t_{NN})^2]}{\int\limits_{s_{\pi\pi}-\Delta s_{\pi\pi}}^{s_{\pi\pi}+\Delta s_{\pi\pi}} ds_{\pi\pi} \sqrt{\frac{s_{\pi\pi}-4\mu^2}{s_{\pi\pi}}}}, \qquad (31)$$

since experimental and simulated data exist for the strip $s_{\pi\pi}^{(\alpha)} - \Delta s_{\pi\pi} \le s_{\pi\pi} \le s_{\pi\pi}^{(\alpha)} + \Delta s_{\pi\pi}$ of the non-negligible width $2\Delta s_{\pi\pi}$ in the plane $(t_{NN}, s_{\pi\pi})$. Analytical calculations result in cumbersome expressions than that of (30), so they are not shown here. Because of the rapid growth of the $\pi\pi$ amplitude with $s_{\pi\pi}$ at the threshold, the difference of the simple function (28) and the above one (31) was found to be reaching the 20% level at $\Delta s_{\pi\pi} = 0.15\mu^2$.

The non-negligent spread in $s_{\pi\pi}$ has another important issue for the extrapolation. The specific bin (α) is then characterized by the rectangle $(t_{NN}^{(\alpha)} \pm \Delta t_{NN}, s_{\pi\pi}^{(\alpha)} + \Delta s_{\pi\pi})$ in the Chew–Low plane $(t_{NN}, s_{\pi\pi})$. The cross section for the bin is given by the integral

$$\sigma_{(\alpha)}(\|M\|^2; t_{NN}) = \int_{s_{\pi\pi}^{(\alpha)} - \Delta s_{\pi\pi}}^{s_{\pi\pi}^{\rm MAX}} ds_{\pi\pi} R(\|M\|^2; s_{\pi\pi}, t_{NN}), \qquad (32)$$

where $R(\|M\|^2; s_{\pi\pi}, t_{NN})$ stands for the matrix element integrated with respect to the rest two variables including the $\pi\pi$ scattering angle. The upper limit,

$$s_{\pi\pi}^{\rm MAX} \equiv {\rm MAX}\{s_{\pi\pi}^{(\alpha)} + \Delta s_{\pi\pi}, s_{\pi\pi}^{+}(t_{NN})\}, \qquad (33)$$

is independent of t_{NN} only for bins (α) such that their intersection with the strip $s_{\pi\pi}^{(\alpha)} - \Delta s_{\pi\pi} \le s_{\pi\pi} \le s_{\pi\pi}^{(\alpha)} + \Delta s_{\pi\pi}$ is located strictly inside the physical domain of the Chew–Low plot. Therefore, when bins are close to the boundaries of the physical interval $[t_{NN}^-(s), t_{NN}^+(s)]$, the physical space in the $s_{\pi\pi}$ variable is limited not by the t_{NN}-independent value $s_{\pi\pi} + \Delta s_{\pi\pi}$ but by the curve

$$\begin{aligned}
s_{\pi\pi}^{+}(t_{NN}) = \frac{1}{2m^2}\big\{&t_{NN}(s + m^2 - \mu^2) + 2m^2\mu^2 + \\
&\sqrt{t_{NN}(t_{NN} - 4m^2)(s - (m+\mu)^2)(s - (m-\mu)^2)}\big\}. \qquad (34)
\end{aligned}$$

As a result, the value of the phase space $\sigma_{(\alpha)}(1; t_{NN})$ for such bins does depend on t_{NN} as well as cross sections $\sigma_{(\alpha)}(\|M\|^2; t_{NN})$ do. This makes it necessary to withdraw such bins from the extrapolation base, regardless of the kind of the extrapolation function. For example, both the cross section $\sigma_{(\alpha)}(\|M\|^2; t_{NN})$ and quasi-amplitude have the breaking points at two values of t_{NN}, for which $s_{\pi\pi}^{+}(t_{NN}) = s_{\pi\pi} + \Delta s_{\pi\pi}$. This phenomenon is clearly seen in Fig. 2. The selection of bins is an easy problem in the course of a practical data treatment. It is solved by calculating the empty phase space for the considered array of bins and keeping on the ones with the constant value of the phase space.

Had the $s_{\pi\pi}$ dependence of the partially integrated matrix element $R(s_{\pi\pi}, t_{NN})$ be known in advance, it would be possible to insert corrections for the bins intersecting the boundary curve $s_{\pi\pi}^{+}(t_{NN})$ and include more points into the Chew–Low extrapolation. Our curves in Fig. 2 are corrected by the empty phase space — evidently this is insufficient. Another possibility to enlarge the base of extrapolation by cutting more narrow strips in $s_{\pi\pi}$ depends on the amount of available experimental events.

4.2 Simulations of the Chew–Low extrapolation

Here, we discuss the simulations of t_{NN} distributions for the fixed strip in $s_{\pi\pi}$ performed at $P_{\rm Lab} = 335$, 420 and 460 MeV/c. Extrapolation functions calculated for three types of theoretical amplitudes are shown in Fig. 2. These data are simulated with the binning and the precision which are only computer-dependent; the same binning of the available experimental data suffers a lack of statistics — this is clearly demonstrated by empty experimental bins in the discussed pictures.

Simulated data are extrapolated to the point $t_{NN} = \mu^2$. The true limiting value for each amplitude is calculated with the use of (31). The linear (*lin*) and the quadratic (*squ*) extrapolation patterns are selected for demonstrations. Extrapolation results are collected in Table 3, where true limiting value specific to the considered amplitudes are given in the bottom boxes. We display here the variation of the extrapolated values with the choice of the left bound $t_{NN,1}$ the right bound $t_{NN,2}$ being fixed.

The *o* columns of Table 3 are the undoubted grounds for the crucial inference that even in the simplified case of

Table 3. Results of the linear (*lin*) and quadratic (*squ*) Chew–Low extrapolations to the point $t_{NN} = \mu^2$ for various left-hand bounds $t_{NN,1}$. The theoretical amplitudes used for the data simulations correspond to: o — the solution with OPE contribution only; g — the solution with all mechanisms; x — the solution with all mechanisms excluding OPE. The quantities given in the bottom boxes show the true values at $t_{NN} = \mu^2$

			$P_{\rm Lab} = 335$ MeV/c, $s_{\pi\pi} = 4.15\mu^2$					
n	$t_{NN,1}/\mu^2$	$t_{NN,2}/\mu^2$	o_{lin}	o_{squ}	g_{lin}	g_{squ}	x_{lin}	x_{squ}
17	−5.519	−1.155	0.6111	0.7889	1.201	0.866	0.1612	0.3578
16	−5.262	−1.155	0.6204	0.7883	1.176	0.909	0.1712	0.3582
14	−4.749	−1.155	0.6382	0.7871	1.138	0.987	0.1898	0.3669
12	−4.235	−1.155	0.6546	0.7892	1.112	1.067	0.2087	0.3723
10	−3.722	−1.155	0.6709	0.7875	1.100	1.140	0.2286	0.3697
8	−3.208	−1.155	0.6858	0.7864	1.099	1.223	0.2479	0.3589
6	−2.695	−1.155	0.6998	0.7096	1.111	1.341	0.2607	0.3953
			0.7870	0.7870	0.6036	0.6036	0.0000	0.0000
			$P_{\rm Lab} = 420$ MeV/c, $s_{\pi\pi} = 4.15\mu^2$					
n	$t_{NN,1}/\mu^2$	$t_{NN,2}/\mu^2$	o_{lin}	o_{squ}	g_{lin}	g_{squ}	x_{lin}	x_{squ}
17	−10.01	−1.283	0.4497	0.7097	0.4011	0.3829	0.4971	0.5755
16	−9.497	−1.283	0.4672	0.7090	0.3848	0.4435	0.4971	0.5965
14	−8.470	−1.283	0.4999	0.7098	0.3715	0.5568	0.5051	0.6259
12	−7.444	−1.283	0.5315	0.7055	0.3838	0.6502	0.5208	0.6395
10	−6.417	−1.283	0.5598	0.7028	0.4154	0.7361	0.5384	0.6496
8	−5.390	−1.283	0.5845	0.7070	0.4632	0.8261	0.5561	0.6688
6	−4.364	−1.283	0.6089	0.6990	0.5321	0.8703	0.5782	0.6715
			0.7054	0.7054	0.4751	0.4751	0.0000	0.0000
			$P_{\rm Lab} = 460$ MeV/c, $s_{\pi\pi} = 4.45\mu^2$					
n	$t_{NN,1}/\mu^2$	$t_{NN,2}/\mu^2$	o_{lin}	o_{squ}	g_{lin}	g_{squ}	x_{lin}	x_{squ}
21	−12.58	−1.797	0.1849	0.4911	−0.0071	0.908	0.2755	1.485
20	−12.06	−1.797	0.2015	0.4916	0.0174	1.006	0.3477	1.462
18	−11.04	−1.797	0.2337	0.4917	0.8569	1.200	0.4837	1.405
16	−10.01	−1.791	0.2643	0.4917	0.1830	1.378	0.6084	1.325
14	−8.984	−1.797	0.2928	0.4933	0.3074	1.535	0.7152	1.230
12	−7.957	−1.797	0.3198	0.4951	0.4568	1.658	0.7997	1.131
10	−6.930	−1.797	0.3459	0.4917	0.6242	1.737	0.8584	1.042
8	−5.904	−1.797	0.3695	0.4895	0.8043	1.726	0.8938	0.969
6	−4.877	−1.797	0.3906	0.4939	0.9711	1.653	0.9096	0.922
			0.4886	0.4886	0.3591	0.3591	0.0000	0.0000

the pure OPE mechanism the linear extrapolation method usually underestimates the value in question and results in a systematic error of 25–35%. The impression of some improvement with the move to the extreme right position in the t_{NN} interval is misleading, since the effect of nonzero errors of the real experimental data must make the result even more ambiguous at the reduced extrapolation base. We must also note that the OPE amplitude (i.e. o) does not fit at all the complete set of data (see Table 4 of the paper [25] for values of χ^2).

There are no advantages of both linear and quadratic extrapolation methods in the more realistic case g, when all mechanisms are present; the coincidence of the results with the exact numbers seems to be of a random nature. The 200–300% deviation makes it unreliable to use both linear and quadratic extrapolations even for estimations.

What is really disappointing is the examination of the columns x. The nonzero numbers give rise to the suspicions that the extrapolations follow the dictate of the experimental data rather than the theoretical amplitude. Indeed, the theoretical amplitude x fits well to the data but *it has no pole at all* at $t_{NN} = \mu^2$.

5 Discussion

In view of the negative general conclusion on the applicability of the Chew–Low extrapolation at the considered energies, we need to shed more light on its origin.

A special explanation is necessary for the pure OPE mechanism, since the application of the Chew–Low approach is based on the hypothesis of the OPE dominance. Indeed, six — eight data points are enough for successful extrapolation, if Nature follows the simplest pattern of

the OPE dominance in the $\pi N \to \pi\pi N$ reaction. A discrepancy displayed in Table 3 is due to different isospin breakings in the main program and extrapolation function (31).

It is not so difficult to realize that the small deviation of the extrapolation function (28) from the linear pattern is due to the participation of the D-wave parameters g_2 and g_3 — see the quantities Φ_{22}, Φ_{23}, Φ_{33} given by (30). If these parameters are absent, the internal integrations of the leading order ChPT amplitude in the formula (28) result in linear function of t_{NN}. The quoted parameters slightly affect the $\pi\pi$ amplitude at the considered energies. Nonlinearity of the extrapolation function is small but it influences the extrapolations drastically.

The off-shell appearance of the $\pi\pi$ amplitude in the $\pi N \to \pi\pi N$ reaction acts the part of the magnification lens in respect to D-wave parameters — we have already seen this in the previous section, when their contributions to the threshold amplitudes were discussed. However, the above phenomenon does not present an obstacle by itself, since the quadratic extrapolation for a pure OPE amplitude is proved to be exact and stable.

It is the complicated form of the $\pi N \to \pi\pi N$ amplitude that excludes the possibility of a reliable application of the Chew–Low extrapolation in the simplest manner. This conclusion is derived in terms of a particular ansatz of the extrapolation function (27). Let us discuss now, why the conclusion is of more general nature.

There is the difference between our function $F_M(t_{NN})$ and the functions defined in terms of cross sections: we are extracting the square root of (27). The quadratic behaviour of the function $F_{\rm OPE}(t_{NN})$ in t_{NN} is equivalent to the fourth-order behaviour of the cross-section form of extrapolation function. The quadratic approximation for the latter function is not good enough. Hence, we see no reason in using the cross-section form. It is not the point which is capable to disapprove our conclusions. So let us discuss another feature implemented in our extrapolation function (27).

There is the property of the pure OPE cross section $\sigma_{|t_{NN}\to 0} = 0$ which was displayed long ago by nonrelativistic calculations (see, for example the textbook by Källen [37]) and by relativistic calculations as well, like that of the paper [35] by Naisse and Reignier. The work [36] by Baton, Laurens and Reignier represented the phenomenological test of this property by the high energy ($P_{\rm LAB} = 2.77$ GeV/c) data; since then, it was inserted into the Chew–Low procedure. Nevertheless, the known failures of applications of the Chew–Low approach were associated with the relying on the very property we are discussing here — see the review [4] by Leksin. More attentive analysis shows that sometimes the foothold for the definition (27) upon the property $\sigma_{|t_{NN}\to 0} = 0$ is the reason of the overshooting of the quadratic extrapolations, accurately following the extrapolated data in the physical region.

Let us now briefly remind what is the theoretical status of the hypothesis $\sigma_{|t_{NN}\to 0} = 0$. Definitely, this is the exact property of the pure OPE mechanism. What value the matrix element $\|\langle\pi_2\pi_3 N(q)|S|\pi_1 N(p)\rangle\|^2$ obtains at $p = q$ is the kinematical problem in part. It should be noted that the point with $p = q$ is located outside the physical region both for the $\pi N \to \pi\pi N$ reaction and for the four-pion vertex, since the condition $p = q$ implies $s_{\pi\pi} = \mu^2$.

The form factor S of the amplitude (4) gets the same factor $(-t_{NN})$ in the unpolarized matrix element (9) as the OPE contribution does. This form factor gives rise to spin-flip amplitudes, which are the only amplitudes for the considered reaction surviving at the threshold. However, besides this form factor, there are three more; kinematically, their contributions to the quantity (9) are determined by the matrix (10).

Thus, to make the matrix element (9) vanish at $p = q$ all entries of the matrix (10) must become zero simultaneously. The analysis of the explicit expressions, for which we have no room here, shows that three conditions are necessary: 1) $s = (m + \sqrt{s_{\pi\pi}})^2$; 2) collinear final pions $k_2 = k_3$; 3) Chiral limit $\mu = 0$. At the same time, the last condition is the only general reason that can make the considered form factors vanish dynamically.

Therefore, in the real dynamics, the quantity $\|M\|^2_{t_{NN}\to 0}(\sigma(t_{NN} = 0))$ stands for expressing the Chiral symmetry breaking that is similar to the πN-elastic Σ term. It oscillates with the energy at least in the region of isobars, but it seems to be rather small. Nevertheless, it prevents from making the safe simplification of the extrapolation function, namely, dividing the quasi-amplitude by $\sqrt{-t_{NN}}$. This can also explain the alternating successes and failures in the application of the Chew–Low procedure at relatively close energies. Thus, we arrive at the conclusion that, from one side, the complicated t_{NN}-dependence of the physical amplitude makes useless the linear and quadratic extrapolation methods, from the other side, the presence of the Chiral symmetry breaking in the true amplitude forbids to soften the t_{NN}-dependence of the extrapolation ansatz.

6 Conclusions

We used the amplitude of the $\pi N \to \pi\pi N$ reaction built of numerous resonance contributions, including the separately treated OPE mechanism, and the smooth polynomial background (see the paper [25]). Its complicated appearance was proved to reflect the influence of numerous processes, like $\pi\pi \to \pi\pi$, $\pi N \to \pi N$, $\pi N \to \pi N^{(*)}$, $\pi N \to \pi\Delta$, on the physics of the near-threshold region. Unknown details of isobar interactions were shown to be the major difficulties encountered within the Oset–Vicente-Vacas approach.

The use of the amplitude fixed by fittings to the vast set of near-threshold data for modelling the Chew–Low extrapolation and Olsson–Turner approach displays that the cause of the difficulties is the same, the effect being stronger.

It is shown that the application of the linear Chew–Low extrapolation cannot be justified either for the cross-section form of the extrapolation function or for the quasi-amplitude one. The extrapolation results in enermous the-

oretical errors, the extracted values being in fact random numbers. The simplification of the extrapolation ansatz is not generally valid, the proof of its pertinence cannot be achieved within the approach.

The results of the Olsson–Turner method are characterized by significant systematic errors coming from unknown details of the isobar physics.

More narrow data base required by the Olsson–Turner and Chew–Low approaches is an advantage of the methods. The consistency analysis of the data base of the Olsson–Turner approach in terms of threshold identities makes it obvious that more narrow data base disproportionally increases the total error.

Anyway, the correct application of the Olsson–Turner approach requires the due account of isobar physics and the precise knowledge of interaction parameters. We conclude that only the approach based upon the extensive phenomenological model (*a là* Oset–Vicente-Vacas) is helpful in investigations of the considered reaction. The investigations require to develop the simultaneous analyses of related processes like $\pi N \to \pi N^{(*)}$, $\pi N \to \pi\Delta$, thus, extending the energy region up to $P_{\rm Lab} \sim 1$ GeV/c. In other words, the problem of determination of the low-energy $\pi\pi$-scattering characteristics is a part of more comprehensive problem of the investigation of $\pi N \to \pi\pi N$ dynamics at low and intermediate energies.

This research was supported in part by the RFBR grant N 95-02-05574a. We thank T.A. Bolokhov, P.A. Bolokhov, A.N. Manashov for checking the formulae, testing the code and for other help at various stages of the project. We are grateful to P. Amaudruz, A. Bernstein, F. Bonutti, J. Brack, P. Camerini, G.A. Feofilov, E. Frlež, N. Grion, G. Hofman, R.R. Johnson, M. Kermani, M.G. Olsson, O.O. Patarakin, M.V. Polyakov, D. Počanić, R. Rui, M. Sevior, G.R. Smith for helpful discussions. We especially thank the CHAOS team for presenting computer powers of ALPHA stations at TRIUMF (Vancouver) and INFN (Trieste).

References

1. Knecht, M., Moussalam, B., Stern, J., and Fuchs, N.H.: Nucl. Phys. B**457**, 513 (1995)
2. Stern, J., Sazdjian, H., and Fuchs, N.H.: Phys. Rev. D: Part. Fields **47**, 3814 (1993)
3. Bijenes, J., Colangelo, G., Ecker, G., Gasser, J., and Sainio, M.A.: Phys. Lett. B**374**, 210 (1996)
4. Leksin, G.A.: Sov. Phys. Uspekhi **102**, 387 (1970)
5. Bolokhov, A.A. and Sevior, M.E.: *Interpretation of $\pi N \to \pi\pi N$ measurements*, in Bernstein, A.M., and Holstein, B.R., (eds.), *Chiral Dynamics: Theory and Experiment, Proceedings of the Workshop held at MIT*, Cambridge, MA, USA, 25–29 July 1994, *Lecture Notes in Physics*, LNP **452**, 115 Berlin and Heidelberg: Springer-Verlag 1995
6. Goebel, C.J.: Phys. Rev. Lett. **1**, 337 (1958); Chew, G.F. and Low, F.E.: Phys. Rev. **113**, 1640 (1959)
7. Grayer, G., et al.: Nucl. Phys. B**75**, 189 (1974)
8. Martin, B.R., Morgan, D., and Shaw, G.: *Pion-Pion Interactions in Particle Physics*, NY: Academic Press 1976
9. Oset, E. and Vicente-Vacas, M.J.: Nucl. Phys. A**446**, 584 (1985)
10. Bolokhov, A.A., Vereshagin, V.V., and Sherman, S.G.: Nucl. Phys. A**530**, 660 (1991)
11. Olsson, M.G. and Turner, L.: Phys. Rev. Lett. **20**, 1127 (1968); Phys. Rev. **181**, 2141 (1969); Phys. Rev. D: Part. Fields **6**, 3522 (1972)
12. Kernel, G., Korbar, D., et al.: Phys. Lett B**225**, 198 (1989)
13. Kernel, G., Korbar, D., et al.: Phys. Lett B**216**, 244 (1989)
14. Kernel, G., Korbar, D., et al.: Z. Phys. C**48**, 201 (1990)
15. Kernel, G., et al.: Z. Phys. C**51**, 377 (1991)
16. Sevior, M.E., Ambardar, et al.: Phys. Rev. Lett. **66**, 2569 (1991)
17. Lowe, J., Bassalleck, B., et al.: Phys. Rev. C: Nucl. Phys. **44**, 956 (1991)
18. Počanić, D., Frlež, E., Assamagan, K.A., et al.: Phys. Rev. Lett. **72**, 1156 (1994)
19. Meissner, Ulf-G.: Rep. Prog. Phys. **56**, 903 (1993)
20. Bernard, V., Kaiser, N. and Meissner, Ulf-G.: Phys. Lett. B**332**, 415 (1994); B**338**, 520 (1994)
21. Pocanic, D.: *Summary of π-π Scattering Experiments*, in Bernstein, A.M., and Holstein, B.R., (eds.), *Chiral Dynamics: Theory and Experiment, Proceedings of the Workshop held at MIT*, Cambridge, MA, USA, 25–29 July 1994, *Lecture Notes in Physics*, LNP **452**, 95 Berlin and Heidelberg: Springer-Verlag 1995
22. *http://helena.phys.virginia.edu/~pipin/E1179/E1179.html*
23. *http://helena.phys.virginia.edu/~pipin/E857/E857.html*
24. Smith, G.R., et al.: Nucl. Instr. and Meth. A**362**, 349 (1995)
25. Bolokhov, A.A., Polyakov, M.V. and Sherman, S.G.: Eur. Phys. J. A**1** (1998) 3, 317–336
26. Review of Particle Physics. Phys. Rev. D: Part. Fields **54**, Number 1 (1996)
27. Aitchison, I.J.R., Brehm, J.J.: Phys. Lett. B**84**, 349 (1979)
28. Burkhardt, H. and Lowe, J.: Phys. Rev. Lett. **67**, 2622 (1991)
29. Počanić, D.: *In Proc. of Conf. Meson and Nuclei at Intermediate Energies, May 3–7, 1994, Dubna*, Dubna: JINR, 1994
30. Beringer, J.: *πN-Newsletter, issn 0942-4148* **7**, 33 (1992)
31. Olsson, M.G., Meissner, Ulf-G., Kaiser, N. and Bernard, V.: *On the interpretation of the $\pi N \to \pi\pi N$ data near threshold*. Preprint CRN 95-13, 1995
32. Bernard, V., Kaiser, N. and Meissner, Ulf-G.: Nucl. Phys. B**457**, 147 (1995)
33. Meissner, Ulf-G.: *The Reaction $\pi N \to \pi\pi N$ at Threshold, Talk given at 7th International Conference on the Structure of Baryons*, Santa Fe, NM, 3–7 Oct. 1995. Preprint TK 95 29, 1995, 4p.; hep-ph/9510390
34. Bernard, V., Kaiser, N. and Meissner, Ulf-G.: *The Reaction $\pi N \to \pi\pi N$ above Threshold in Chiral Perturbation Theory*. Preprint KFA-IKP(TH)-1997-05, Mar. 1997, 29p.; hep-ph/9703218
35. Naisse, and J., Reignier, J.: Fortschritte der Physik **12**, 523 (1964)
36. Baton, J.P., Laurens, G. and Reignier, J.: Nucl. Phys. B**3**, 349 (1967)
37. Källen, G.: *Elementary Particle Physics*, London: Addison-Wesley Publishing company, Inc. 1964
38. Blokhintseva, T.D., Kravtsov, A.V., et al.: Yad. Fiz. **12**, 101 (1970); Sov. Journ. Nucl. Phys. **12**, 55 (1971)